

A PARALLAX-BASED DISTANCE ESTIMATOR FOR SPIRAL ARM SOURCES

M. J. Reid¹, T. M. Dame¹, K. M. Menten², A. Brunthaler²

ABSTRACT

The spiral arms of the Milky Way are being accurately located for the first time via trigonometric parallaxes of massive star forming regions with the BeSSeL Survey, using the Very Long Baseline Array and the European VLBI Network, and with the Japanese VERA project. Here we describe a computer program that leverages these results to significantly improve the accuracy and reliability of distance estimates to other sources that are known to follow spiral structure. Using a Bayesian approach, sources are assigned to arms based on their (l, b, v) coordinates with respect to arm signatures seen in CO and H I surveys. A source's kinematic distance, displacement from the plane, and proximity to individual parallax sources are also considered in generating a full distance probability density function. Using this program to estimate distances to large numbers of star forming regions, we generate a realistic visualization of the Milky Way's spiral structure as seen from the northern hemisphere.

Subject headings: Galaxy: structure – parallaxes – stars: formation

1. Introduction

The Bar and Spiral Structure Legacy (BeSSeL) Survey ³ and the Japanese VLBI Exploration of Radio Astrometry (VERA) ⁴ are now supplying large numbers of trigonometric parallaxes to sites of massive star formation across large portions of the Milky Way. Since

¹Harvard-Smithsonian Center for Astrophysics, 60 Garden Street, Cambridge, MA 02138, USA

²Max-Planck-Institut für Radioastronomie, Auf dem Hügel 69, 53121 Bonn, Germany

³<http://bessel.vlbi-astrometry.org>

⁴<http://veraserver.mtk.nao.ac.jp>

massive star forming regions (MSFRs) are excellent tracers of spiral structure in galaxies, these parallax distances allow one to construct a sparsely sampled map of the spiral structure of the Milky Way (Honma et al. 2012; Reid et al. 2014). This map can be used to characterize spiral arms, even if they are somewhat irregular (Honig & Reid 2015), and to provide a predictive model for the locations of other sources that *a priori* are likely to reside in arms, such as H II regions, giant molecular clouds (GMCs), and associated infrared sources.

In this paper we describe a computer program and web-based application for estimating distances to spiral arm sources based solely on their Galactic longitude and latitude coordinates and local standard-of-rest velocities: $(l, b, v)_{\text{src}}$. In many cases, one can use a source’s $(l, b, v)_{\text{src}}$ coordinates to confidently assign it to a portion of a spiral arm, based on its proximity to $(l, b, v)_{\text{arm}}$ traces of spiral arms seen in CO or H I surveys. Since distances to large sections of arms are now known (Xu et al. 2013; Zhang et al. 2013; Choi et al. 2014; Sato et al. 2014; Wu et al. 2014; Hachisuka et al. 2015; Xu et al. 2016), this can lead to an accurate and reliable distance estimate. We also add information from a kinematic model, Galactic latitude, and proximity to individual giant molecular clouds for which parallax distances have been measured. Since spiral arms are not circular, but wind outward from the Galactic center with pitch angles between about 7° and 20° (Reid et al. 2014), arm location and kinematic distance information can be complementary. We combine all of this information, using a Bayesian approach similar to that introduced by Ellsworth-Bowers et al. (2013) for resolving kinematic distance ambiguities, to estimate a probability density function (PDF) for source distance.

Details of the distance PDF calculation are given in Section 2 and some example PDFs are discussed in Section 3. In Section 4, we compare our program’s performance on a sample of H II regions thought to be very distant based on H I absorption information. In Section 5, we estimate distances of large numbers of spiral arm sources from Galactic plane surveys to provide a visualization of the Milky Way, which includes realistic distributions of star formation activity. Finally, the Appendix displays the Galactic (l, v) plots, used to determine the $(l, b, v)_{\text{arm}}$ traces for spiral arms, which are central to determining distance PDFs.

2. Bayesian Distance Estimation

Measurements of parallaxes of masers in massive star forming regions allow one to reliably trace the locations of spiral arms in the Milky Way. Since spiral arms can be clearly identified as continuous curves in $(l, b, v)_{\text{arm}}$ traces of H I (Weaver 1970) or CO (Cohen et al. 1980) emission, one can often assign an individual source to a spiral arm based solely

on its $(l, b, v)_{\text{src}}$ coordinates. Thus, combining the locations of spiral arms, from parallax measurements, with assignment to an arm, any source that is associated with spiral arms can be located in the Milky Way in three-dimensions with some degree of confidence.

In addition to spiral arm assignment, there is other information available that indicates distance, including kinematic distance, Galactic latitude, and location within a giant molecular cloud with a measured parallax. These types of distance information are subject to uncertainty in varying ways and can best be combined in a Bayesian approach. We employ this information by constructing a PDF for each type of distance information and then multiplying them together to arrive at a combined distance PDF. With simplified notation, the probability density that a source is at a distance d is given by

$$\text{Prob}(d) \propto \text{Prob}_{SA}(d) \times \text{Prob}_{KD}(d) \times \text{Prob}_{GL}(d) \times \text{Prob}_{PS}(d) \quad ,$$

where the subscripts indicate different types of distance information (*SA*: spiral arm model; *KD*: kinematic distance; *GL*: Galactic latitude; *PS*: parallax source) as detailed below.

We fit the combined distance PDF with a model of a flat background probability density and multiple Gaussian components, estimating their peak probability densities, locations (i.e., distances), and widths (i.e., distance uncertainties). The total probability of each component is calculated by integrating its Gaussian probability density over distance. Note that the component with the greatest integrated probability may not have the greatest probability *density*, since a tall, narrow Gaussian can have less area than a short, wide Gaussian. The program reports the component with the greatest integrated probability, and up to two more components if significant.

The BeSSeL Survey website (<http://bessel.vlbi-astrometry.org>) provides a web-based application that generates distance PDF plots similar to those in Section 3. We also make available the FORTRAN program, which allows for more efficient use on large catalogs of star forming sources. Also available are the detailed spiral arm (l, b, v, R, β, d) traces used by the program. In addition to the Galactic longitude, latitude and LSR velocities of the arm segments, they include current best estimates of the Galactocentric radii (R), azimuths (β ; defined as 0 toward the Sun and increasing clockwise as viewed from the North Galactic Pole), and heliocentric distances (d).

2.1. Spiral Arm PDF

Key distance information is provided by the locations of spiral arm segments in the Galaxy, which are based largely on trigonometric parallaxes of high mass star forming regions. As mentioned above, we compare a target source's $(l, b, v)_{\text{src}}$ with traces of an arm

segment’s $(l, b, v)_{\text{arm}}$ values to estimate the probability that the source is associated with an arm segment. In the Appendix, we provide some background for the identification of spiral arms in (l, v) plots and a description of the (l, b, v) traces, which we determined from CO and H I data.

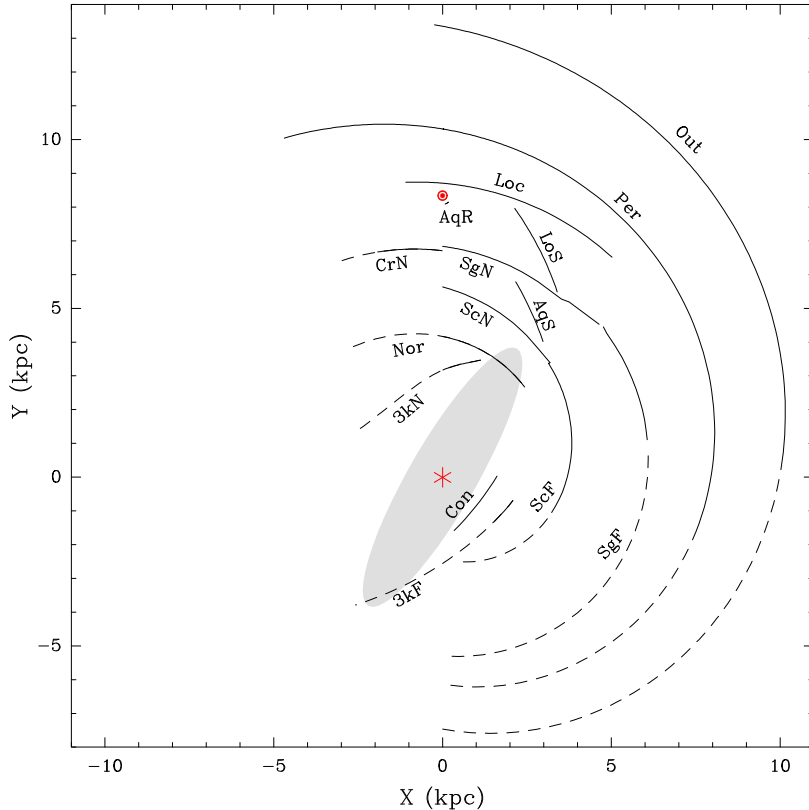


Fig. 1.— Locations and forms of spiral arm segments in the Milky Way as determined from trigonometric parallaxes of water and methanal masers (Reid et al. 2014, and references therein) associated with HMSFRs (*solid lines*). *Dashed lines* indicate extrapolations based on fits of log-periodic spiral forms to the parallax data. Arm segments are labeled as follows: Outer (Out), Perseus (Per), Local (Loc), Carina near portion (CrN), Sagittarius near and far portions (SgN, SgF), Scutum near and far portions (ScN, ScF), Norma or 4-kpc (Nor), 3-kpc near and far arms (3kN, 3kF), and Connecting (Con). Also shown are other features including the Aquila Rift (AqR), Aquila Spur (AqS), and the Local spur (LoS). The Outer Scutum-Centaurus (OSC), Carina far (CrF), an extension of Connecting (CnX), and Centaurus-Crux near and far (CtN and CtF) arm segments currently have no parallax measurements and are not plotted. The Galactic Center and Sun are indicated with a *red asterisk* and *red Sun symbol*.

We used the fits of log-periodic spiral shapes to arm segments (slightly updated with some unpublished data) from the values summarized in Reid et al. (2014) to define the location of each arm segment (see Fig. 1). For any given Galactic longitude, we calculated the arm’s Galactocentric radius and azimuth, R and β , and the heliocentric distance, d , and

combined this information with the arm $(l, b, v)_{\text{arm}}$ trace, to generate complete 6-parameter information, (l, b, v, R, β, d) , for all arm segments. For the Aquila Spur, Aquila Rift, and Connecting arm, distances were estimated from only one or two parallaxes using simple linear forms. The (l, b, v, R, β, d) information for 20 arm segments are currently used by the program, and we plan to update these and add new arm segments when more parallax data is available.

We calculate a distance PDF, based on spiral arm information, as the product of the probability density of distance to arm segments, based on models fitted to parallax data and other information, and the probability of association with those arm segments:

$$\text{Prob}_{SA}(d|l, b, v, I) = \sum_{j=1}^J \text{Prob}(d|\text{arm}_j, l, b, v, I) \times \text{Prob}(\text{arm}_j|l, b, v, I) \quad ,$$

where I indicates prior information on the locations of J spiral arm segments, as well as Galactic (R_0 , Θ_0 , rotation curve) and Solar Motion (U_\odot , V_\odot) parameters. We assign the probability that a source resides in the j^{th} arm segment as follows:

$$\text{Prob}(\text{arm}_j|l, b, v, I) = e^{-\Delta l_j^2/2\sigma_{l_j}^2} e^{-\Delta b_j^2/2\sigma_{b_j}^2} e^{-\Delta v_j^2/2\sigma_{v_j}^2} \quad ,$$

where Δl_j , Δb_j , and Δv_j are the minimum deviations in longitude, latitude, and velocity of the source from the center of the $(l, b, v)_{\text{arm}}$ trace for the j^{th} spiral arm, respectively, and σ_{l_j} , σ_{b_j} , and σ_{v_j} are their expected dispersions.

The in-plane and out of plane dispersions are given by $\sigma_{l_j} = \sigma_s \sec \alpha / d_{\text{arm}_j}$ and $\sigma_{b_j} = \sigma_z / d_{\text{arm}_j}$, respectively, where σ_s and σ_z are the in-plane and out of plane widths (Gaussian 1σ) of an arm, and α is the angle between the tangent to the arm and a ray from the Sun through the target source. The $\sec \alpha$ term accounts for the increased “effective” width of the arm owing to its orientation with respect to its closest approach to the target ray. Since real arms curve over kpc-scale lengths, we truncate $\sec \alpha$ above a value of 10.

Both σ_s and σ_z can be a function of Galactocentric distance. Reid et al. (2014) found that spiral arm width increases with Galactocentric radius, R , with a slope of 42 pc kpc^{-1} for $R > 5 \text{ kpc}$. Rather than extrapolate this to zero width near $R = 0$, we adopt $\sigma_s = 0.14 + 0.042(R - 4) \text{ kpc}$ for $R > 4 \text{ kpc}$ and constant at $\sigma_s = 0.14 \text{ kpc}$ in the central 4 kpc as shown in Fig. 2. In order to estimate the z -width, we grouped the same parallax data by spiral arm and calculated the standard deviations about their mean offsets in z . These are also plotted in the figure. The z -widths are consistent with increasing for $R > 8 \text{ kpc}$ with the same slope as for the in-plane widths, and we adopt a simple broken-linear relation $\sigma_z = 0.04 + 0.042(R - 8) \text{ kpc}$ for $R > 8 \text{ kpc}$ and 0.04 kpc inside of 8 kpc. Finally, we set

$\sigma_{v_j} = \sqrt{2} \sigma_{\text{vir}}$, which is the expected Virial 1-dimensional speed *difference* for the target and a giant molecular cloud used to define the spiral arm $(l, b, v)_{\text{arm}}$ trace. We adopt $\sigma_{\text{vir}} = 5 \text{ km s}^{-1}$, which is appropriate for $\sim 10^6 M_{\odot}$ within $\sim 100 \text{ pc}$.

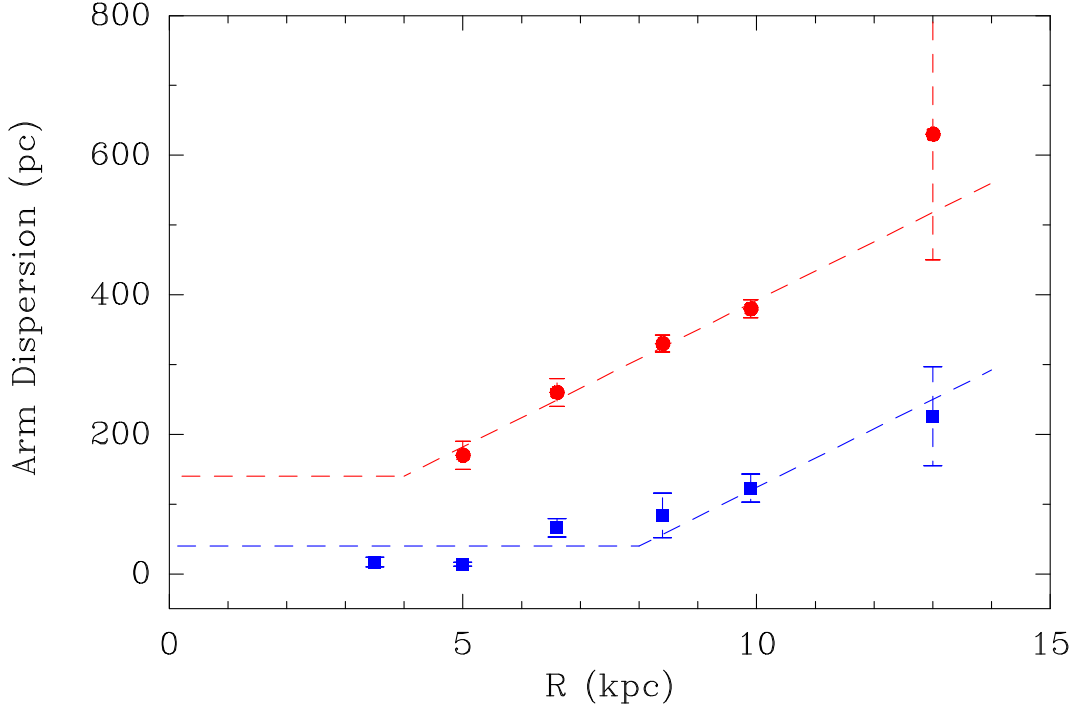


Fig. 2.— Spiral arm dispersion in width (*red circles*) and z-height (*blue squares*) versus Galactocentric radius after Reid et al. (2014). Data from parallax sources were assigned to spiral arms and for each arm’s data we calculated and plotted the standard deviation about the mean against the average radius. *Dashed lines* indicate broken linear fits, that were used to determine the expected deviations of sources from the model spiral arm segments.

In order to calculate $\text{Prob}(d|\text{arm}, l, b, v, I)$, we generate an array of “trial” source distances, d , and calculate the minimum separation of the source from a given arm segment model, both in the Galactic plane, Δs , and out of the plane, Δz . Then for the j^{th} arm,

$$\text{Prob}(d|\text{arm}_j, l, b, v, I) \propto \frac{1}{\sigma_s} e^{-\Delta s^2/2\sigma_s^2} \frac{1}{\sigma_z} e^{-\Delta z^2/2\sigma_z^2} ,$$

where the arm in-plane and z-widths are σ_s and σ_z . Note, we include the “normalization” terms, $1/\sigma_s$ and $1/\sigma_z$, preceding the exponentials, since they vary with distance.

Since the sum of the probabilities of association with arms

$$S = \sum_{j=1}^J \text{Prob}(\text{arm}_j|l, b, v, I)$$

can be small, we add a uniform background probability that allows for the possibility of a missing arm segment in our model and to some extent interarm sources (but see Section 5 for caveats). A user-adjustable parameter, P_{SA} from $0 \rightarrow 1$, determines the maximum weighting of the spiral arm associations relative to the background probability. When normalizing the PDF, we set the total background probability (i.e., integrated over distance) to be $1 - \min(S, P_{SA})$. Thus, for example, if $S = 0$, indicating zero probability of the target being associated with spiral arms, then the background probability would integrate to unity, regardless of the value assigned to P_{SA} . However, if $S \geq 1$, indicating a high probability that the source can be assigned to one or more arms, then the spiral arm PDF will be downweighted such that the background probability density would integrate to $1 - P_{SA}$. The program defaults to $P_{SA} = 0.5$.

2.2. Kinematic Distance PDF

The kinematic distance PDF, $\text{Prob}_{KD}(d)$, is generated for a given distance based on the velocity difference between the observed value and that expected from the rotation of the Galaxy. First, we calculate a “revised LSR velocity” to allow for differences between the Standard Solar Motion (which defines LSR velocities) and more recent estimates. We convert LSR to the Heliocentric velocities by removing the IAU Standard Solar Motion of 20 km s^{-1} toward R.A.= 18^h , Dec.= 30° (in 1900 coordinates), which when precessed to J2000 give Cartesian Solar Motion components of $(U_\odot^{Std}, V_\odot^{Std}, W_\odot^{Std}) = (10.27, 15.32, 7.74) \text{ km s}^{-1}$. Then we calculate the revised LSR velocity by applying (user-supplied) updated $(U_\odot, V_\odot, W_\odot)$ values. Interestingly, the IAU recommended values are surprisingly close to what could be considered today’s best values, and for simplicity the results in this paper adopt the IAU values.

Next, we obtain the velocity difference, Δv , between the revised LSR velocity and that expected from the rotation of the Galaxy. Rather than use a simple linear rotation curve, we adopt the “Universal” rotation curve formulation of Persic, Salucci & Stell (1996) as implemented by Reid et al. (2014) (see their Figure 4 and Table 5 for details). This formulation is well motivated by observations of other galaxies, and it produces a nearly flat curve for Galactocentric radii $\gtrsim 5 \text{ kpc}$ and slower rotation for sources inside that radius, in agreement with parallax and proper motion results.

Assuming an individual star in a high-mass star forming region has a random (Virial) motion of $\sigma_v = 5 \text{ km s}^{-1}$ in one dimension, we calculate the distance PDF via

$$\text{Prob}_{KD}(d|l, v, \sigma_v, I) \propto \frac{1 - e^{-r^2/2}}{r^2/2} \quad ,$$

where $r = \Delta v / \sigma_v$. We have used the Sivia & Skilling (2006) “conservative formulation” for the distance PDF, because it admits much higher probability for large deviations from the kinematic distance than would a Gaussian distribution. This is critical as it better approximates the true probability density from kinematic information, which can have large systematic errors owing to significant peculiar motions. See Section 3 for an example of an aberrant kinematic distance. Note that by directly generating a PDF, we have avoided calculating a traditional “kinematic distance,” which can have many complications when a velocity uncertainty is allowed.

For some sources, one may have prior information on the probability that the source is beyond the tangent point, near the far distance. For example, if H I absorption is seen toward an H II region with speeds exceeding that of the region by $\gtrsim 20 \text{ km s}^{-1}$, one can be fairly confident that the source distance is past the tangent point. (Although, there are places in the Galaxy where hydrogen gas has large non-circular motions that can lead to anomalous absorption velocities.) A user-supplied parameter, P_{far} , giving the prior probability (from 0 to 1) that the source is at the far distance, is used to weight the near and far PDFs before they are summed and normalized. When no such prior information is available, $P_{far} = 0.5$, and both near and far kinematic distance PDFs are given equal weight.

2.3. Galactic Latitude PDF

A source’s Galactic latitude, b , is a direct indicator of distance, independent of spiral arm association, since the $\text{Prob}(d|b)$ is taller and narrower for a more distant source than for a near one. From Bayes’ theorem, the distance PDF can be calculated from

$$\text{Prob}(d|b, \sigma_z, I) = \frac{\text{Prob}(b|d, \sigma_z, I)\text{Prob}(d|\sigma_z, I)}{\text{Prob}(b|\sigma_z, I)} .$$

Neither $\text{Prob}(d|\sigma_z, I)$ nor $\text{Prob}(b|\sigma_z, I)$ introduce distance terms and converting from latitude to z -height gives

$$\text{Prob}(b|d, \sigma_z, I) \propto \text{Prob}(z|d, \sigma_z, I) \frac{\partial z}{\partial b} .$$

Since $\partial z / \partial b = d$ and for a Gaussian distribution in z , we find

$$\text{Prob}(d|b, \sigma_z, I) \propto d e^{-z^2/2\sigma_z^2} .$$

The above formula is valid for a flat Galaxy. Allowing for a Galactic warp, we replace z in the above relation with the *difference*, Δz , between a source’s Galactic height z ($= d \times b$) and a model of the Galaxy’s warp. Rather than adopt a mathematical formula for warping,

we use the spiral arm (l, b, v, R, β, d) traces and calculate the z -height of each arm segment at the intersection of the arm with a ray from the Sun through a target source position. At any given distance from the Sun, we then estimate the z -height of the Galactic “plane” by interpolating (or extrapolating) linearly between (d, z) pairs of arm-warp parameters. Typically, we obtain 2 or 3 such (d, z) -pairs in the 2nd and 3rd quadrants and 4 to 6 pairs in the 1st quadrant. In order to evaluate the PDF, we use the broken-linear relation for σ_z presented in Section 2.1

2.4. Parallax Sources PDF

Sources with measured parallaxes have provided most of the information used to fit segments of spirals that are included in our prior knowledge (I), although other information (such as tangent-point longitudes) can be included in the models. However, adopting a log-periodic spiral model for arm segments $\gtrsim 5$ kpc in length can be a simplification, and there is residual information in the parallax measures (e.g., star formation substructure and deviation of the real arm from the mathematical model) which we would like to use. So, we calculate a distance PDF based on association of the target source with a parallax source, $\text{Prob}_{PS}(d)$, as the product of the probability of distance given a parallax source, determined by its parallax accuracy, times the probability of association, given (l, b, v) information for both the target and the parallax source. Summing over K parallax sources gives

$$\text{Prob}_{PS}(d|l, b, v, I) = \sum_{k=1}^K \text{Prob}(d|PS_k, l, b, v, I) \times \text{Prob}(PS_k|l, b, v, I) .$$

We quantify the association of a target source with a parallax source by calculating the probability that they reside within the same giant molecular cloud (GMC), based on the separations in linear distance in longitude ($\Delta d_l = d\Delta l$) and latitude ($\Delta d_b = d\Delta b$) and in velocity (Δv):

$$\text{Prob}(PS_k|l, b, v, I) \propto e^{-\Delta d_l^2/2\sigma_{GMC}^2} e^{-\Delta d_b^2/2\sigma_{GMC}^2} e^{-\Delta v^2/2\sigma_{\Delta v}^2} ,$$

where we set the expected 1-dimensional separation of two sources within a GMC to be $\sigma_{GMC} = 0.05$ kpc and the expected separation in line-of-sight velocity to be $\sigma_{\Delta v} = \sqrt{2} \sigma_{\text{Vir}} \approx 7$ km s⁻¹ .

For the k^{th} source with measured parallax, $p \pm \sigma_p$, we calculate

$$\text{Prob}(d|PS_k, I) \propto p^2 e^{-\Delta p^2/2\sigma_p^2} ,$$

where for a given distance d , $\Delta p = (1/d) - p$. Note, since what is measured is parallax, not distance, we have employed $\text{Prob}(d) = \text{Prob}(p) \times p^2$ in the PDF calculation. Owing to the possibility of multiple parallax sources (possibly from different spiral arms) having similar (l, b, v) values as the target source, we limit the impact of this probability term by adding a constant background probability density to $\text{Prob}_{PS}(d|l, b, v, I)$ based on the cumulative weight of the parallax matches:

$$W_\pi = \sum_{k=1}^K \text{Prob}(PS_k|l, b, v, I) \ .$$

A user-adjustable parameter, P_{PS} from $0 \rightarrow 1$, determines the maximum weighting of the parallax source association relative to the background probability. When normalizing the PDF, we set the total background probability integrated over distance to be $1 - \min(W_\pi, P_{PS})$. (See the discussion in Section 2.1.) In light of the partial correlation of individual parallax source information with that in the spiral arm model, the program defaults to a moderately-low weighting of this information by setting $P_{PS} = 0.25$.

3. Example Distance PDFs

We present examples of the distance PDFs for sources in the 1st and 2nd Galactic quadrants. G019.60–00.23 is a star formation water maser at $v = 47 \text{ km s}^{-1}$ from the Valdetaro et al. (2001) catalog and its distance PDF is shown in Fig. 3. This source was found to have a high probability of association with the near portion of the Scutum arm at a distance of 3.3 kpc and lower probabilities of association with the Norma arm at 5.3 kpc and the far portion of the Sagittarius arm at 12.9 kpc. Both the near kinematic distance and the association with a parallax source (G018.87+00.05) strongly favor the near Scutum arm distance. Combining all information, G019.60–00.23 is estimated to be at a distance of $3.38 \pm 0.18 \text{ kpc}$ in the near portion of the Scutum arm with an integrated probability of 95% (and a 5% probability at $12.62 \pm 0.32 \text{ kpc}$ in the far portion of the Sagittarius arm).

G136.84+01.12 is a 6.7 GHz methanol maser source at $v = -45 \text{ km s}^{-1}$ in the Pestalozzi, Minier & Booth (2005) catalog, and its distance PDF is shown in Fig. 4. This source has a very high probability of association with the Perseus spiral arm (which crosses the source’s longitude at a distance of $\approx 2.4 \text{ kpc}$). It may be associated with a giant molecular cloud containing the parallax source (G133.95+1.05) near the inner edge of the arm. The kinematic distance for G136.84+01.12 is 3.7 kpc, which, if correct, would place it in the Outer spiral arm. However, this portion of the Perseus arm is well known for kinematic anomalies, and the program correctly recognizes that the source $(l, b, v)_{\text{src}}$ values are inconsistent with Outer arm

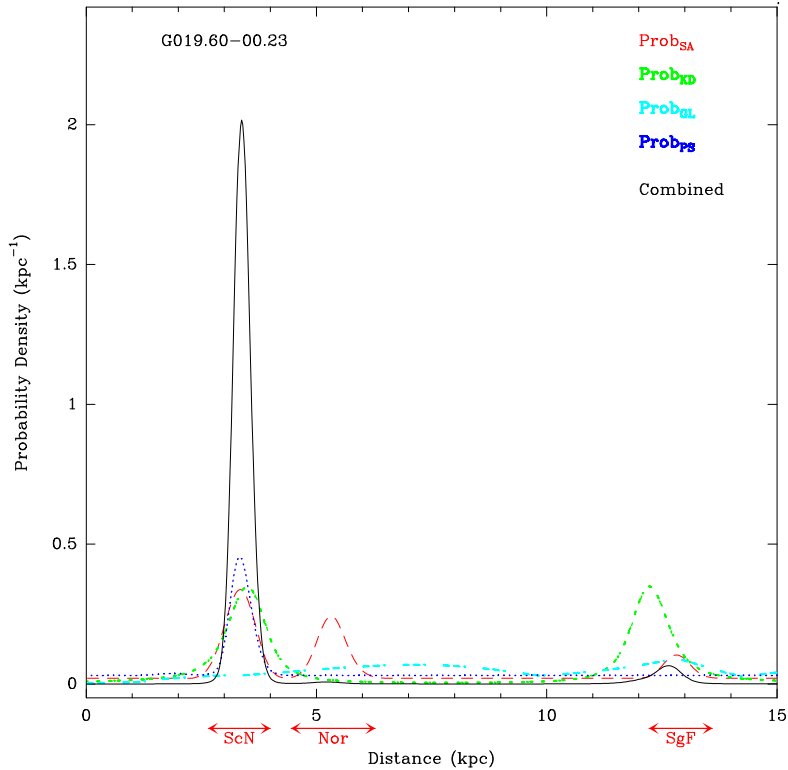


Fig. 3.— Distance probability density function for G019.60–00.23, a 22 GHz water maser at $v = 47 \text{ km s}^{-1}$ from the Valdetaro et al. (2001) catalog. The $(l, b, v)_{\text{src}}$ values most likely associate it with the near portion of the Scutum spiral arm (at 3.3 kpc), although the Norma arm (at 5.4 kpc) and the far portion of the Carina-Sagittarius arm (at 12.9 kpc) are not ruled out (*red dashed lines*). However, the combination (*solid black line*) of arm assignment probability with the kinematic distance (*green dot-dashed line*), latitude probability (*cyan dashed line*) and association with a parallax source (*blue dotted line*) strongly favor a distance of $3.38 \pm 0.19 \text{ kpc}$.

values. This is an example of the utility of a non-Gaussian PDF (see Section 2) for kinematic distances, as it accommodates such anomalies. The program favors a distance of $1.96 \pm 0.04 \text{ kpc}$ (based on the very accurate parallax to a nearby source) over a slightly greater distance of $2.36 \pm 0.27 \text{ kpc}$ (from the arm mid-line), as is apparent from an examination of the PDF.

4. Comparisons with Other Distance Estimates

A common method to estimate distances to Galactic sources of star formation is to use kinematic distances, augmented by H I absorption spectra to resolve the near/far ambiguity for sources within the Solar circle. Recently, Anderson et al. (2012) discovered large numbers of H II regions in the 1st quadrant, and for most they resolved the distance ambiguity via H I

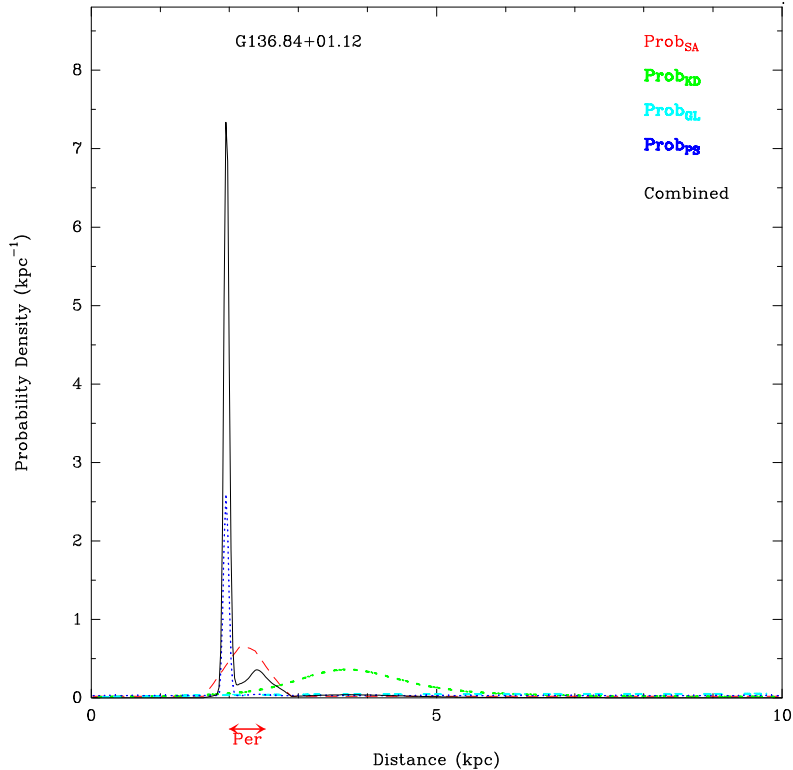


Fig. 4.— Distance PDF for G136.84+01.12, a 6.7 GHz methanol maser at $v = -45 \text{ km s}^{-1}$ from the Pestalozzi, Minier & Booth (2005) catalog. The $(l, b, v)_{\text{src}}$ values associate it with the Perseus spiral arm centered near 2.4 kpc (*red dashed line*). This information, coupled with association with the parallax source G133.95+1.05 (*blue dotted line*), favors the distance estimate of 1.96 ± 0.04 kpc over the arm center. Note that the kinematic distance (*green dot-dashed line*) suggests a much greater distance of 3.7 kpc, as it does for many sources in this part of the Perseus arm which is known to be kinematically anomalous.

absorption. They found 62 sources that could be confidently (“A-grade”) placed at the far kinematic distance. Using our Bayesian approach with no prior information to resolve the near/far ambiguity (i.e., $P_{\text{far}} = 0.5$), we were able to assign distances with 90% or greater probability for 34 of these sources. Of these sources, there was agreement between the H I absorption and our technique as to the resolution of the near/far distance ambiguity for all but six sources.

The techniques disagree for two sources near 19° longitude. For G018.324+0.026 and G019.662–0.305, the Bayesian approach finds a significantly more probable association with the near portion of the Scutum arm at a distance of 3.4 kpc than with the far portion of the Sagittarius arm at 13 kpc. Similarly, we find G029.007+0.076 is likely associated with the near portion of the Scutum arm at a distance of ≈ 4 kpc, whereas at the far kinematic distances of ≈ 11 kpc there are no probable arm associations. If these sources are at the

distances suggested by our Bayesian program, then they are near the end of the Galactic bar and may have significant non-circular motions, which could confuse distances based on kinematics and H I absorption.

For the remaining three sources (G032.272–0.226, G034.041+0.053 and G034.133+0.471) we find them likely associated with the near portion of the Sagittarius arm at ≈ 2.1 kpc rather than at the far kinematic distance of ≈ 12 kpc. Note that along our line of sight toward longitude $\approx 34^\circ$ there may be gas with anomalous velocities owing to interaction with the supernova remnant W 44 (centered at $(l, b) = (3469, -041)$ with a radius of 06) or with winds from its precursor.

Even though our program suggests a near distance for these six sources with greater than 90% probability, that still leaves a non-negligible probability for an alternative distance. All in all, we conclude that when a source can be assigned to a spiral arm with high probability, there is generally good agreement between our Bayesian approach and using H I absorption to resolve the near/far distance ambiguity.

5. The Milky Way’s Spiral Structure

One application of our Bayesian distance estimation program is to generate a “plan view” (i.e., a projected view from high above the plane) of the spiral structure of the Milky Way. The left panel of Fig. 5 shows the locations of ≈ 2000 HMSFRs, assembled by combining catalogs of water (Valdettaro et al. 2001) and methanol (Pestalozzi, Minier & Booth 2005) masers, HII regions (Anderson et al. 2012), and “red” MSX sources (Urquhart et al. 2014) sources. The distance to each source was determined from the component fitted to the combined distance PDF that had the greatest integrated probability. On the right-hand portion of this figure, where spiral arm locations are established by parallaxes, approximately 90% of the catalog sources are found to be associated with a spiral arm (indicated by the dark blue dots); the remaining approximately 10% probably represent interarm star formation (indicated by the light cyan dots). Since we do not yet have sufficient parallax measurements to locate spiral arms in the southern hemisphere (left-hand portion this figure), distance estimation there is based only on kinematics and latitude. The limitations of kinematic distances, including being multi-valued in the 4th quadrant and having variable sensitivity to non-circular motion, blur the spiral structure in this part of the Milky Way.

In the right panel of Fig. 5 we present a visualization of the Milky Way. For each catalog source we “sprinkle” five dots to simulate multiple sites of star formation in each giant molecular cloud. These dots were shifted from the catalog source location by adding

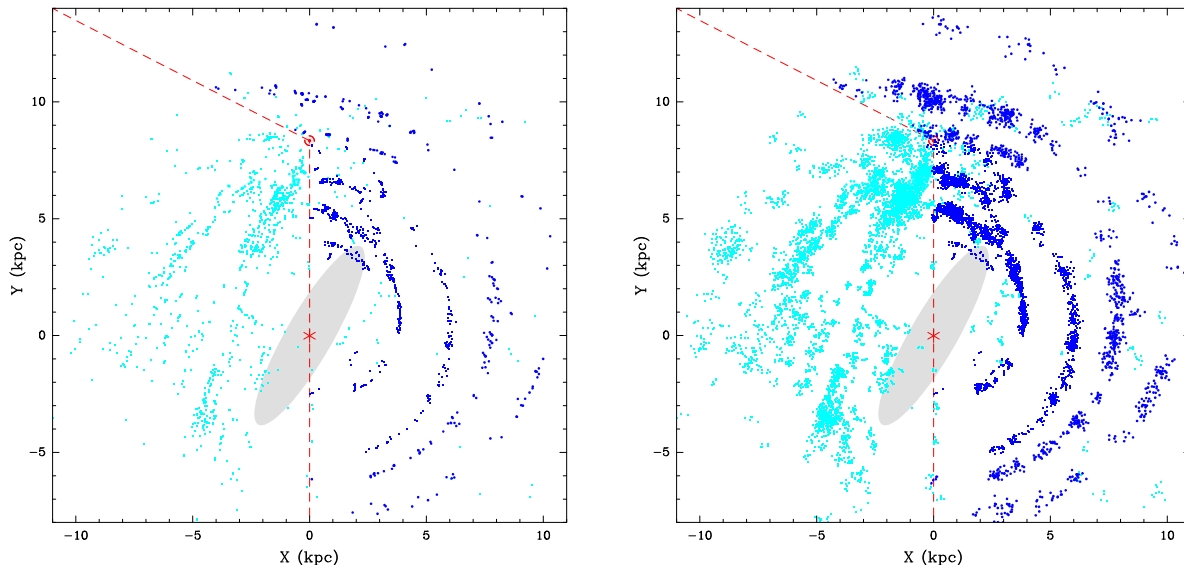


Fig. 5.— *Left Panel:* Map of high-mass star forming regions that trace spiral structure in the Milky Way viewed from the North Galactic Pole. Distances were determined with the Bayesian approach described in this paper, which combines spiral arm locations, association with giant molecular clouds that include sources with measured parallaxes, kinematic distance and Galactic latitude information. Input catalogs included water and methanol masers, HII regions, and “red” MSX sources. *Dark blue dots* indicate sources associated with spiral arms, while the lighter *cyan dots* could not be confidently associated with any arm. The *dashed red lines* separate the regions of the Milky Way mapped with northern hemisphere telescopes (*right side*) from that yet to be mapped with southern hemisphere telescopes (*left side*). The shaded ellipse provides a schematic indication of the Galactic bar. *Right Panel:* Same as the left panel, except that each catalog source is represented by 5 “dots,” spread randomly about the estimated position using a Gaussian kernel with $\sigma = 100$ pc to better represent multiple sources of star formation in a giant molecular cloud. Spiral arms evident in the figures, starting from near the Galactic center and moving outward, are the Norma, Scutum, Sagittarius, Local, Perseus, and Outer arms.

Gaussianly distributed shifts with $\sigma = 100$ pc along each axis. The visualization suggests a clumpy spiral structure with depressions or gaps in massive star forming regions. The dearth of points in the Perseus arm between Galactic longitudes of 50° to 80° , pointed out by Zhang et al. (2013) based on the lack of parallax sources, is apparent, even though the Bayesian distance estimation has no bias against portions of a spiral arm. The Outer and Sagittarius arms also show two or more gaps, several kpc in length.

The assumptions that go into, and the limitations of, Fig. 5 deserve discussion. Firstly, the accuracy of this figure directly depends on the locations of spiral arms, based on parallax results. Currently, the location of the Outer arm at Galactic longitudes $\lesssim 70^\circ$, the Perseus and Sagittarius arms at longitudes $\lesssim 40^\circ$, and the Scutum arms at longitudes $\lesssim 25^\circ$ are extrapolations based on pitch angles fitted to parallax sources at greater longitudes. Since

spiral arms may have pitch angles that vary with azimuth (Honig & Reid 2015), distances to sources in the extrapolated longitude ranges should be considered tentative, pending more parallax data.

Secondly, even though we include a flat (non-zero) background probability density in the spiral arm PDF (see Section 2.1 for details), including $\text{Prob}_{SA}(d)$ in the combined distance PDF will “pull” peaks of combined probability density toward an arm center. To demonstrate this, we generated a uniform grid of sources that follow circular Galactic orbits, and estimate distances to these test sources. In order to simplify this demonstration, the test sources were placed exactly in the Galactic plane and the Galactic latitude, $\text{Prob}_{GL}(d)$, and parallax source, $\text{Prob}_{PS}(d)$, contributions to the combined distance PDF were ignored. The results of this uniform grid test are shown in Fig. 6. In regions of this uniform mock “Galaxy,” where spiral arm information is lacking, the grid is reasonably well preserved. However, where the spiral arm information exists and is used in the combined distance PDF, the results are biased to arms. This highlights the effects of the assumption made in the Bayesian distance estimation method that sources whose $(l, b, v)_{\text{src}}$ values are similar to the $(l, b, v)_{\text{arm}}$ values of a known spiral arm segment probably are in that arm. Therefore, one should not use this method for sources that are not, or only weakly, associated with spiral structure, such as populations of old stars or diffuse gas.

This work was partially funded by the ERC Advanced Investigator Grant GLOSTAR (247078).

Facilities: VLBA, VERA, EVN

REFERENCES

- Anderson, L. D., Bania, T. M., Balsaer, D. S. & Rood, T. 2012 ApJ, 754, 62
- Benjamin, R. A. 2008, in “Massive Star Formation: Observations Confront Theory,” ASP Conference Series, Vol. 387, eds. H. Beuther, H. Linz & Th. Henning, p. 375
- Blitz, L. & Spergel, D. N. 1991, ApJ, 379, 631
- Choi, Y. K., Hachisuka, K., Reid, M. J., et al. 2014, ApJ, 790, 99
- Cohen, R. S., Cong, H., Dame, T. M. & Thaddeus, P. 1980, ApJ, 239, L53

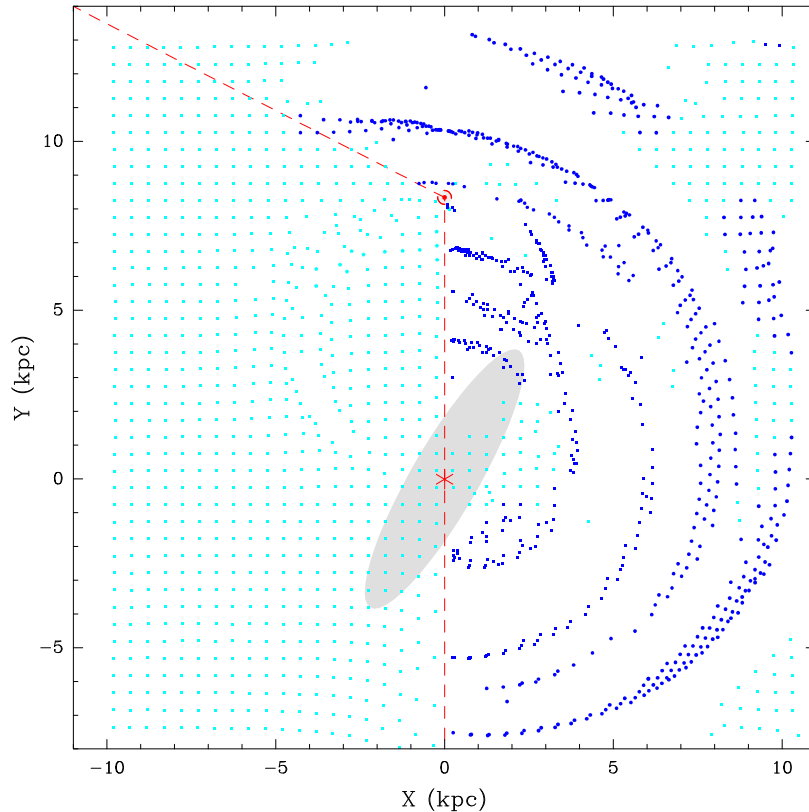


Fig. 6.— Test of the influence of including the spiral arm contribution to the combined distance PDF. We generated fake sources on a uniform grid with pure circular rotation. For sources to the left and below of the *red dashed lines*, where no spiral arm information is used, the program returns the input locations with reasonable accuracy (except for slight deviations in regions near $\ell \approx 0$ and near the “tangent points” where small velocity changes result in large changes in distance). However, to the right and above the *red dashed lines*, spiral arm information was used, resulting in distance estimates biased to spiral arms.

Dame, T. M., Elmegreen, B. G., Cohen, R. S. & Thaddeus, P. 1986, *ApJ*, 305, 829

Dame, T. M. & Thaddeus, P. 2008, *ApJ*, 683, L143

Ellsworth-Bowers, T. P., Glenn, J., Rosolowsky, E. et al. 2013, *ApJ*, 770, 39

Hachisuka, K., Choi, Y. K., Reid, M. J., et al. 2015, *ApJ*, 800, 2

Honma, M., Nagayama, T., Ando, K. et al. 2012, *PASJ*, 64, 136

Honig, Z. N. & Reid, M. J. 2015, *ApJ*, 800, 53

Jackson, J. M., Rathborne, J. M., Shah, R. Y. et al. 2006, *ApJS*, 163, 145

McClure-Griffiths, N. M.; Dickey, J. M., Gaensler, B. M. et al. 2012, *ApJS*, 199, 12

- Persic, M., Salucci, P. & Stel, F. 1996, MNRAS, 281, 27
- Pestalozzi, M. R., Minier, V., Booth, R. S. 2005, A&A, 432, 737
- Reid, M. J., Menten, K. M., Zheng, X. W. et al. 2009, ApJ, 700, 137
- Reid, M. J., Menten, K. M., Brunthaler, A. et al. 2014, ApJ, 783, 130
- Sato, M., Wu, Y. W., Immer, K., et al. 2014, ApJ, 793, 72
- Sivia, D. & Skilling, J. 2006, Data Analysis: A Bayesian Tutorial (2nd ed.; New York, Oxford Univ. Press), 168
- Stil, J. M., Taylor, A. R., Dickey, J. M. et al. 2006, AJ, 132, 1158
- Urquhart, J. S., Figura, C. C., Moore, T. J. T., Hoare, M. G., Lumsden, S. L. et al. 2014, MNRAS, 437, 1791
- Valdettaro, R., Palla, F., Brand, J., et al. 2001, A&A, 368, 845
- Weaver, H. 1970, IAU Symposium 38, “The Spiral Structure of Our Galaxy”, Eds. W. Becker & G. I. Contopoulos, (Dordrecht, Reidel), p.126
- Wu, Y. W., Sato, M., Reid, M. J., et al. 2014, A&A, 566, 17
- Xu, Y., Li, J. J., Reid, M. J., et al. 2013, ApJ, 769, 15
- Xu, Y., Reid, M. J., Dame, T. M. et al. , in preparation
- Zhang, B., Reid, M. J., Menten, K. M. et al. (2013), ApJ, 775, 79

6. Appendix

In Figs. 7–16 we optimally display and trace the numerous arcs and loops in HI 21 cm and CO (l, v) diagrams that have long been recognized as Galactic spiral arms (Weaver 1970; Cohen et al. 1980). These features were used by the BeSSeL Survey to assign high mass star forming regions with measured parallaxes to spiral arms, and they can likewise be used for any spiral arm tracer with a measured velocity by our program. While some of the features are very obvious (e.g., the Perseus arm in the second quadrant; Fig. 8), others are less so

owing to blending with unrelated emission either at the opposite kinematic distance in the inner Galaxy or at other latitudes. For instance, the Far 3-kpc Arm (Dame & Thaddeus 2008) can only be seen clearly in an (l, v) diagram integrated over a very narrow range of latitude near the plane (see Fig. 14). Other features are not only narrow in latitude but are offset from the plane and may even vary in latitude as a function of both longitude and velocity (e.g., the Outer Scutum-Centaurus arm; Fig. 10). Details on how the (l, v) diagrams were produced to best display each arm are given in the captions.

All of the spiral arm tracks, indicated by the colored lines in the figures, roughly correspond in shape and alignment with those expected for segments of logarithmic spiral arms, but we do not fit the features in that way, nor do we extrapolate or link up tracks in regions where they are not clearly seen. Rather, we run the tracks through the actual emission features that define the arms in longitude, latitude, and velocity. In some cases this results in a jaggedness that is slightly subjective, but they are the tracks of the actual spiral arms in the raw spectral-line data, and they are the structures that are now being located accurately in the Galaxy for the first time using maser parallaxes. How or whether these structures link up into a grand design spiral pattern is not relevant for the present purpose.

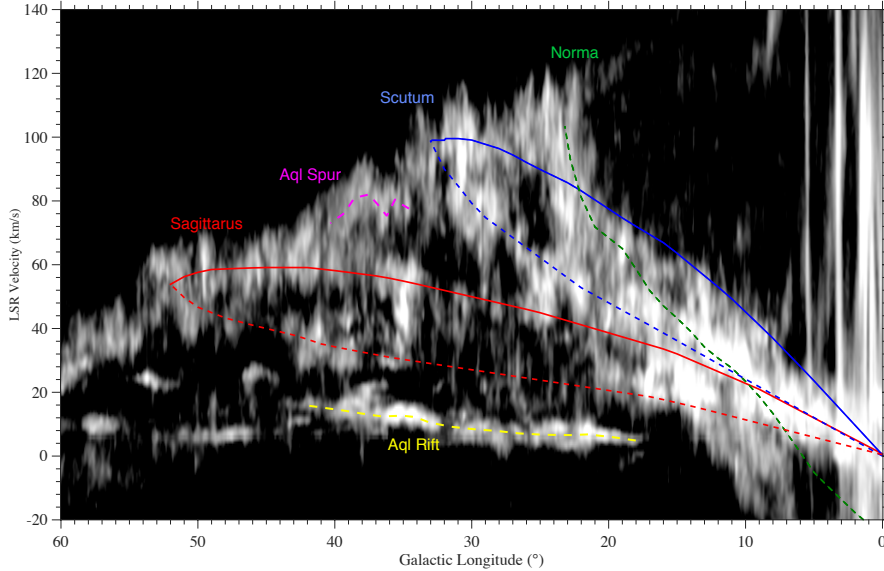


Fig. 7.— Traces of the Sagittarius, Scutum, and Norma arms in the first Galactic quadrant, as well as the smaller Aquila spur (Cohen et al. 1980; Dame et al. 1986) and Aquila Rift features, on the CfA CO survey integrated from $b = -1^\circ$ to $+1^\circ$. The near and far sides of the arms are *dotted* and *solid* lines, respectively. The far side of Scutum probably does not extend below $l \sim 20^\circ$. The near side of the Sagittarius arm passes so close to the Sun that its tracing clouds are widely separated in longitude.

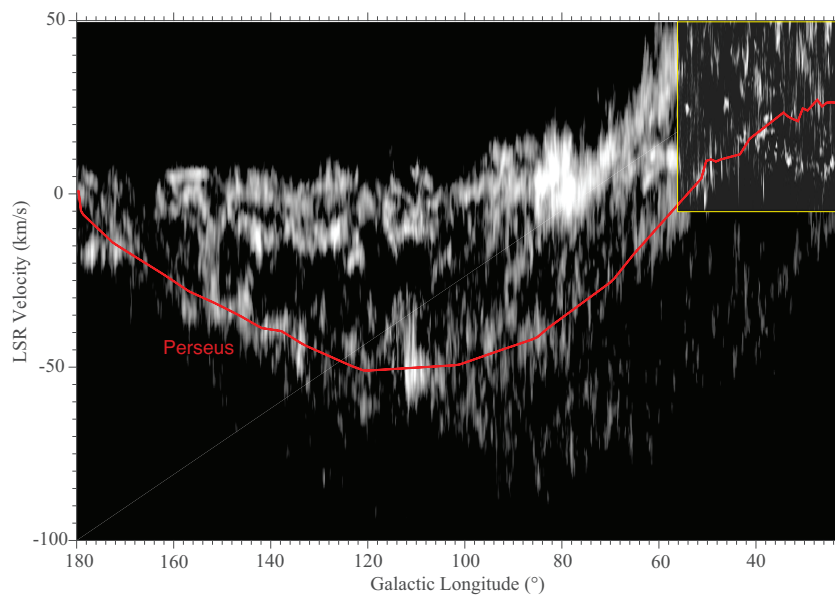


Fig. 8.— A trace of the Perseus arm in the first and second quadrants. Over the longitude range $l = 56^\circ$ to 180° the trace follows the CfA CO survey integrated from $b = -2^\circ$ to $+2^\circ$. At lower longitudes (within the yellow box) the arm spirals into the far side of the inner Galaxy, where its large distance (≈ 12 kpc) and confusion with near-side emission at the same velocity make the arm difficult to follow. In that region, the higher-resolution CO Galactic Ring Survey (Jackson et al. 2006) is integrated over a half-degree strip of latitude that roughly follows the arm in latitude as judged by visual examination of 21-cm latitude-velocity maps from the VGPS survey (Stil et al. 2006).

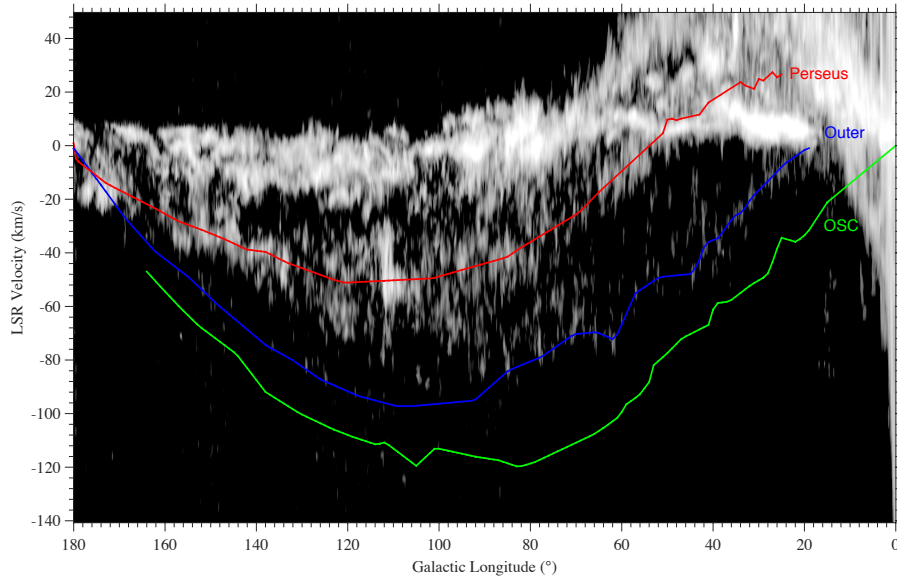


Fig. 9.— A trace of the Outer arm on the CfA CO survey integrated from $b = -5^\circ$ to $+5^\circ$. The survey was moment masked to suppress noise while integrating over such a large range of latitude. The traces of the Perseus and Outer Scutum-Centaurus arms are also shown for reference; note that the CO map here does not show those two arms optimally (see instead Figs. 8 & 10). The emission near -70 km s^{-1} between $l = 65^\circ$ and 100° may be a bridge between the Perseus and Outer arms.

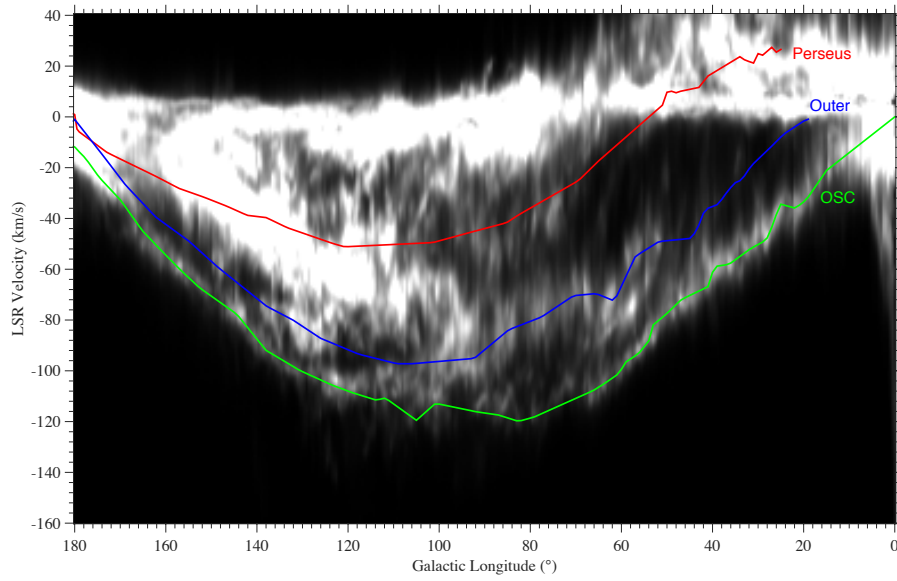


Fig. 10.— A trace of the Outer Scutum-Centaurus arm on the Leiden-Argentine-Bonn 21cm survey integrated over a 1° strip of latitude that roughly follows the arm. The traces of the Outer and Perseus arms are also shown for reference; note that this 21-cm map does not show those two arms optimally.

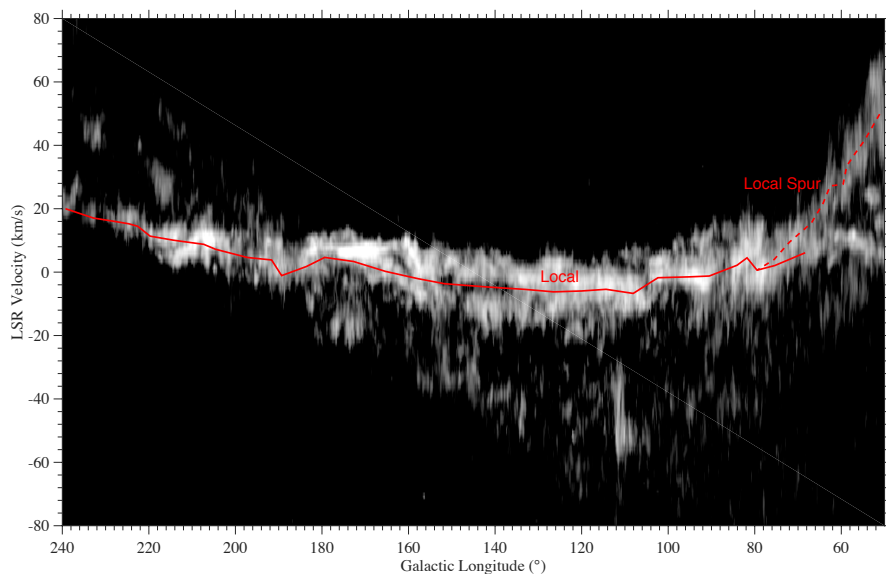


Fig. 11.— Traces of the Local arm and a high-inclination spur that apparently stretches from the Local arm to the region of the Sagittarius arm tangent point (near $l = 50^\circ, v = 60$ km/s). The spur is traced by about six high mass star forming regions with maser parallax distances (Xu et al. in preparation) as well as by CO. The underlying grayscale is the CfA CO survey integrated from $b = -30^\circ$ to $+30^\circ$; the wide latitude range emphasizes nearby material. Both traces closely follow the (l, v) loci defined in Xu et al.

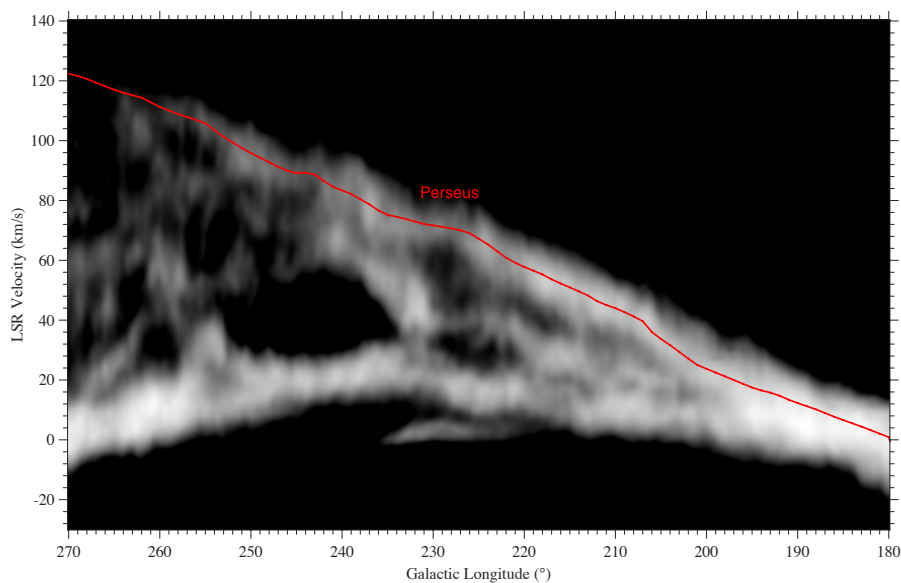


Fig. 12.— A trace of the Perseus arm in the third Galactic quadrant on the Leiden-Argentine-Bonn 21-cm survey integrated from $b = -5^\circ$ to $+2^\circ$.

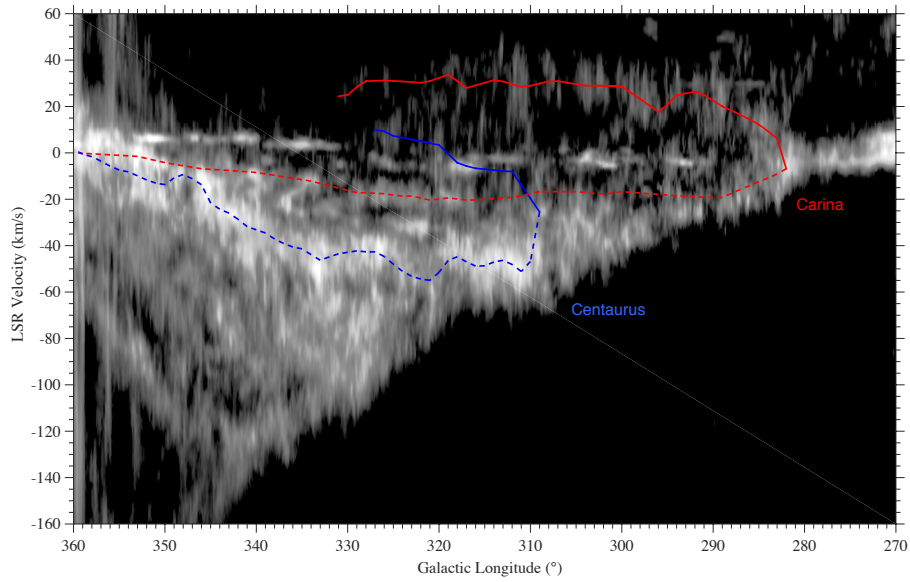


Fig. 13.— Traces of the Centaurus and Carina arms on the CfA CO survey integrated from $b = -5^\circ$ to $+5^\circ$. The survey was moment masked to suppress noise while integrating over such a large range of latitude. The near and far sides of the arms are *dotted* and *solid* lines, respectively. The near side of Carina passes so close to the Sun that its tracing clouds are widely separated in longitude. The far side of Centaurus arm is difficult to trace owing to its great distance (~ 14 kpc).

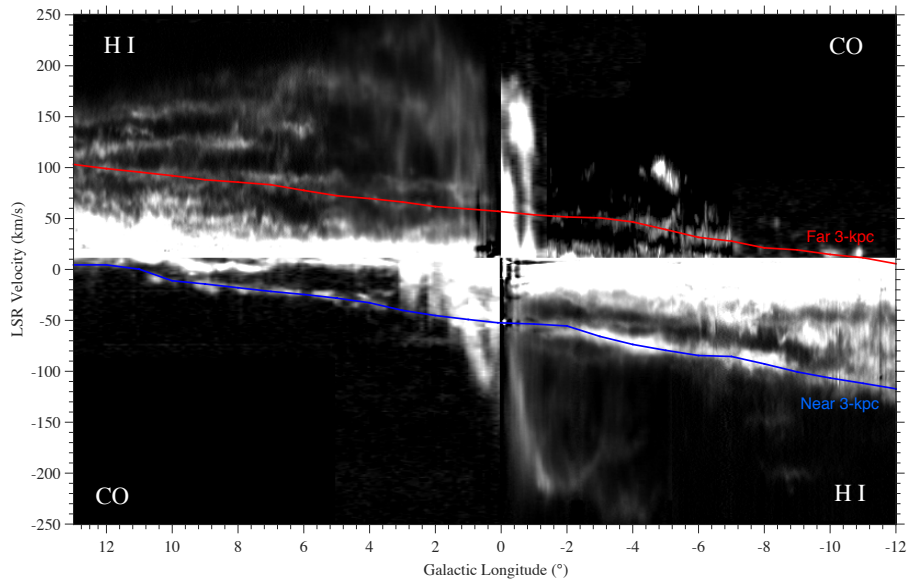


Fig. 14.— A composite of CO and H I surveys near $b = 0^\circ$ tracing the Near and Far 3-kpc arms. The Far 3-kpc arm is best traced in CO at negative longitudes, where it is closer to the far end of the bar and apparently richer in molecular gas; in H I this section of the arm is badly blended with H I emission from the foreground and outer disks. The mirror situation holds for the Near 3-kpc arm; it being best traced by CO at positive longitude and by H I at negative longitudes. The CO data are from the CfA survey, except in the range $l = -1.4^\circ$ to -7° , where high-resolution observations with the Mopra telescope are used (Dame & Barnes, private communication). The H I is from the SGP 21-cm survey of McClure-Griffiths et al. (2012). The CfA survey CO emission is at $b = 0^\circ$, while the higher resolution Mopra and SGP survey data are averaged over a strip of latitude roughly equal to the CfA beam of 8 arcmin.

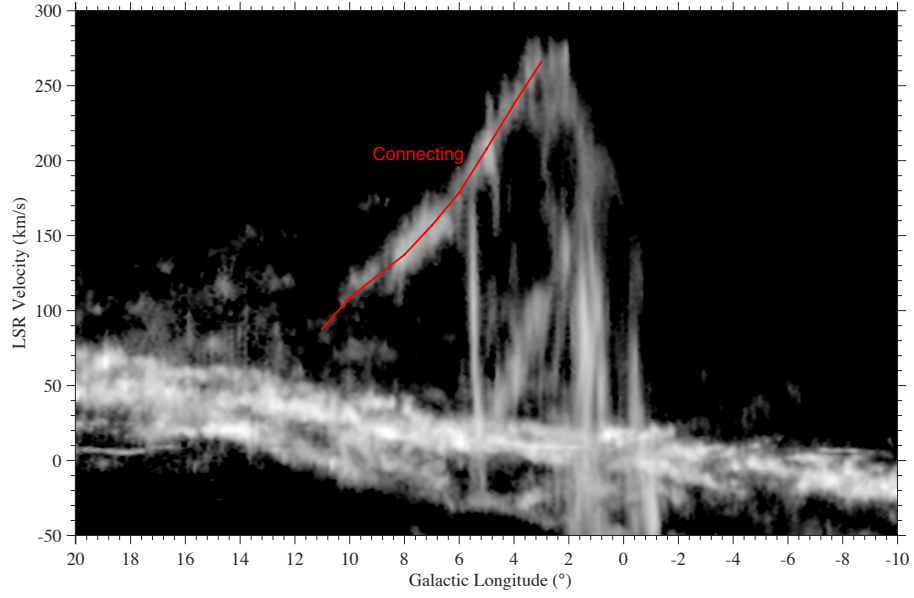


Fig. 15.— A trace of the Connecting arm on the CfA CO survey integrated from $b = -1.25^\circ$ to -0.25° .

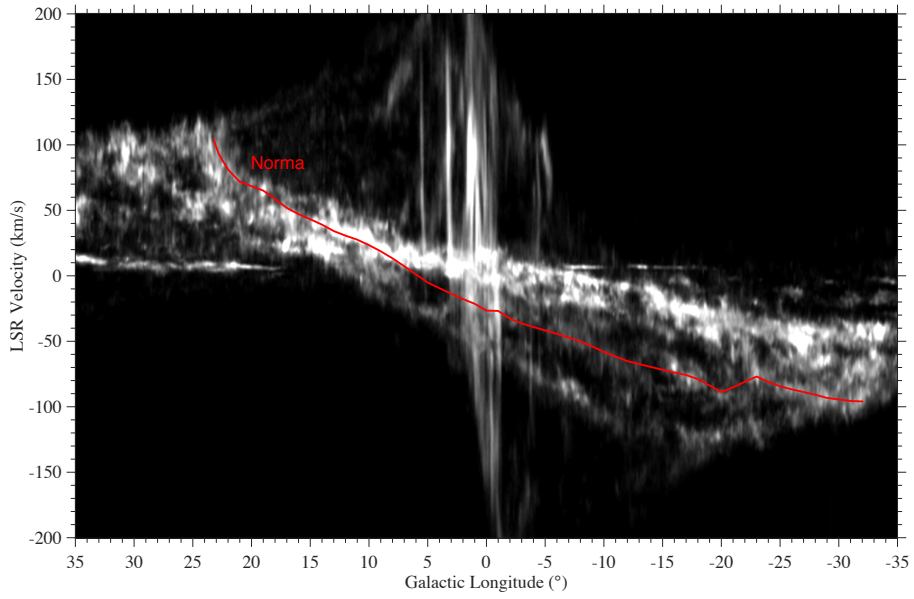


Fig. 16.— A trace of the Norma arm on the CfA CO survey integrated from $b = -1^\circ$ to $+1^\circ$.